TOPICAL REVIEW — Plasmoincs and metamaterials

Manipulating electromagnetic waves with metamaterials: Concept and microwave realizations*

He Qiong(何 琼)[a], Sun Shu-Lin(孙树林)[b], Xiao Shi-Yi(肖诗逸)[a], Li Xin(李 欣)[a], Song Zheng-Yong(宋争勇)[a], Sun Wu-Jiong(孙午炯)[a], and Zhou Lei(周 磊)[a]†

[a] *State Key Laboratory of Surface Physics and Key Laboratory of Micro and Nano Photonic Structures (Ministry of Education), Fudan University, Shanghai* 200433, *China*

[b] *Department of Optical Science and Engineering, and Shanghai Ultra-Precision Optical Manufacturing Engineering Center, Fudan University, Shanghai* 200433, *China*

(Received 3 December 2013; published online 20 February 2014)

Our recent efforts in manipulating electromagnetic (EM) waves using metamaterials (MTMs) are reviewed with emphasis on 1) manipulating wave polarization and transporting properties using homogeneous MTMs, 2) manipulating surface-wave properties using plasmonic MTMs, and 3) bridging propagating and surface waves using inhomogeneous meta-surfaces. For all these topics, we first illustrate the physical concepts and then present several typical practical realizations and applications in the microwave regime.

Keywords: metamaterials, inhomogeneous meta-surface, polarization control, light–matter interaction

PACS: 78.67.Pt, 41.20.Jb, 42.25.Ja, 42.15.Dp **DOI:** 10.1088/1674-1056/23/4/047808

1. Introduction

Metamaterials (MTMs) are artificial electromagnetic (EM) materials comprising a functional subwavelength microstructure (usually called "meta-atoms") arranged in some specific macroscopic order, which can in principle exhibit arbitrary values and even distributions of effective permittivity and effective permeability.[1,2] Compared to ordinary, naturally existing media, MTMs exhibit a much-expanded parametric freedom, which opens new ways to control light and EM waves in a desired manner and leads to many fascinating phenomena.[3–21] Historically, the development of the MTM research is along two lines, namely, the meta-atom and the macroscopic orders. Earlier studies mainly focused on the meta-atom part, by simply assuming the MTMs to possess periodic or homogeneous orders. Even with MTMs with simple orders, lots of fascinating effects were discovered via designing meta-atoms with appropriate EM properties, such as negative refraction,[3,4] superlensing,[5,6] and optical magnetism.[7] On the other hand, people gradually realized the importance of order in expanding the light–manipulation ability of an MTM, due to the establishment of transformation optics (TO) theory[8,9] and related phenomena that were discovered,[10] such as invisibility cloaking,[11,12] illusion optics,[13,14] and TO-based functional devices.[15–17] Very recently, researchers began to work on inhomogeneous MTMs with more fascinating macroscopic orders, particularly a class of planar meta-surfaces (ultra-thin MTM layers) with tailored EM responses, which exhibit even stronger abilities to control light propagations. Via utilizing abrupt local phase changes for EM waves passing through or reflected by the meta-surfaces, more fascinating light–manipulation effects were discovered, such as anomalous light reflection/reflection,[18,19] conversion of a propagating wave to a surface wave with very high efficiency,[20–24] flat lenses to focus EM waves,[25,26] EM-wave helicity control,[27] optical spin hall effect,[28] and so on.

In this paper, we briefly review our recent work on EM manipulation with MTMs along the lines of meta-atoms and macroscopic orders. We follow the logical line of model–realization–application to introduce our work, focusing on both the physical concept behind the discovered phenomena and the practical realizations in the microwave regime. This review will cover three main topics. In Section 2, we describe our recent efforts on manipulating the propagating properties of EM waves using homogenous MTMs, such as polarization control (Subsection 2.1) and transparency manipulation (Subsection 2.2). Section 3 contains our efforts of using plasmonic microwave MTMs to control surface plasmon polariton (SPP) behavior and several related applications. In Section 4, we summarize our recent work on controlling wave-fonts with inhomogeneous meta-surfaces, especially on linking the propagating waves and surface waves by using carefully designed gradient meta-surfaces. Finally, we conclude this review in

*Project supported by the National Natural Science Foundation of China (Grant Nos. 60990321, 11174055, and 11204040), the Program of Shanghai Subject Chief Scientist, China (Grant No. 12XD1400700), the Ministry of Education of China (Grant No. B06011), and the China Postdoctoral Science Foundation (Grant Nos. 2012M520039, 2013T60412).

†Corresponding author. E-mail: phzhou@fudan.edu.cn

© 2014 Chinese Physical Society and IOP Publishing Ltd

Section 5.

2. Manipulating propagating properties of EM waves using homogenous MTMs

2.1. Polarization control

Polarization is an important characteristic of EM waves and its efficient control is highly desired in the views of both science and applications. Conventional methods to manipulate light polarization, such as using optical gratings, birefringent crystals, dichroic crystals, and wire-grid polarizers, inevitably suffer the problems of energy loss and/or size issues for low frequency applications.

MTMs with extraordinary EM properties offer us a new possibility to realize the highly efficient polarization control. Starting from 2007, our group has undertaken a series of efforts to resolve the two main problems faced by the conventional approaches, namely, how to control EM wave polarizations using ultra-thin MTMs with 100% efficiency. The key idea is to fully utilize the much-expanded parametric freedoms in MTMs to create large transmission/reflection phase differences for EM waves polarized along two principle axes. In what follows, we will introduce two typical examples working in reflection and transmission geometries, respectively.

2.1.1. Reflection geometry

In 2007, we proposed an anisotropic metamaterials plate to manipulate the polarization states of EM waves in reflection geometry, and we showed that all possible polarization-conversions are realizable via adjusting the material parameters.[29] In particular, both experiments and simulations demonstrated that a linearly polarized beam can be completely converted to a cross-polarized one when reflected by the anisotropic MTMs under certain conditions.

As shown in Fig. 1(a), the model system consists of an anisotropic homogeneous MTM layer with a dispersive relative permeability tensor $\boldsymbol{\mu}_2$ (with diagonal elements $\mu_{xx}, \mu_{yy}, \mu_{zz}$) and a relative permittivity ε_2 on the top of a perfect metal substrate (with $\varepsilon_3 \to -\infty$, $\mu_3 = 1$). We performed the numerical calculations based on the transfer-matrix method (TMM),[30] assuming that $\varepsilon_2 = 1$, $\mu_{zz} = 1$, $d = 1.3$ mm, $\mu_{xx} = 1 + 70/(12.71^2 - f^2)$, and $\mu_{yy} = 1 + 22/(6.80^2 - f^2)$, where f denotes the frequency measured in units of GHz. Supposing the incident wave is s-polarized, $\boldsymbol{E}_{\rm in} = \hat{\boldsymbol{e}}_{\rm s}^{(\rm i)} \, {\rm e}^{{\rm i}(-\boldsymbol{k}_{\rm i}\cdot\boldsymbol{r}+\omega t)}$, the reflected wave can then be written as $\boldsymbol{E}_{\rm r} = \left(r_{\rm ss}\hat{\boldsymbol{e}}_{\rm s}^{(\rm r)} + r_{\rm sp}\hat{\boldsymbol{e}}_{\rm p}^{(\rm r)}\right) {\rm e}^{{\rm i}(-\boldsymbol{k}_{\rm r}\cdot\boldsymbol{r}+\omega t)}$, where $\hat{\boldsymbol{e}}_{\rm s}^{(\rm i)}$, $\hat{\boldsymbol{e}}_{\rm s}^{(\rm r)}$, and $\hat{\boldsymbol{e}}_{\rm p}^{(\rm r)}$ are the unit E vectors for an incident s-polarized wave, a reflected s-polarized wave, and a reflected p-polarized wave, respectively. We define a polarization conversion ratio (PCR), $R_{\rm PC} = r_{\rm sp}^2/(r_{\rm ss}^2 + r_{\rm sp}^2)$, which measures the energy portion transformed from the original s mode to the p one after the reflection. Without absorption and diffractions, we get $r_{\rm ss}^2 + r_{\rm sp}^2 \equiv 1$, due to energy conservation, and thus $R_{\rm PC} = r_{\rm sp}^2$. The calculated results of $R_{\rm PC}$ are shown as solid lines in Fig. 2(a) for a normal incidence case with $\phi = 45°$, and in Fig. 2(b) for $\theta = \phi = 45°$. We find the PCR to be strongly enhanced around two frequencies, ~ 12.7 GHz, ~ 6.8 GHz, corresponding precisely to the two resonances at which μ_{xx} or μ_{yy} tends to infinity. In particular, for the normal incidence case studied in Fig. 2(a), the theoretical 100% the PCRs at the two resonance frequencies indicate that a linearly polarized light converts its polarization completely after the reflection.

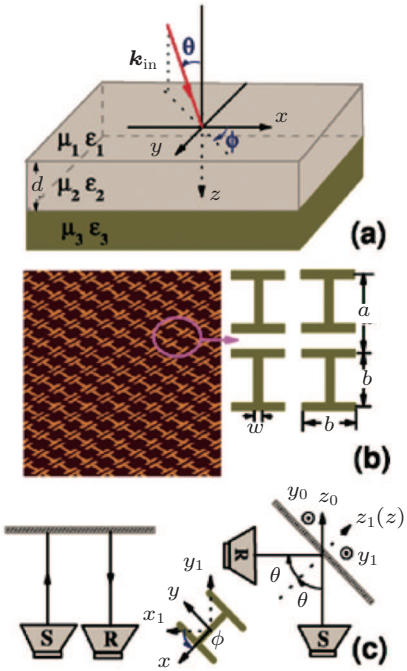


Fig. 1. (a) Geometry of the model system studied. (b) Image of part of the experimental sample. (c) A schematic picture of the experiment setup. Starting from the laboratory coordinate system $\{\hat{x}_0, \hat{y}_0, \hat{z}_0\}$, we first rotate the sample for an angle of θ with respect to the $\hat{y}_0$ $(= \hat{y}_1)$ axis, then for an angle of φ with respect to the $\hat{z}_1 (= \hat{z})$ axis, and finally arrive at the local coordinate system $\{\hat{x}, \hat{y}, \hat{z}\}$ attached to the sample.[29]

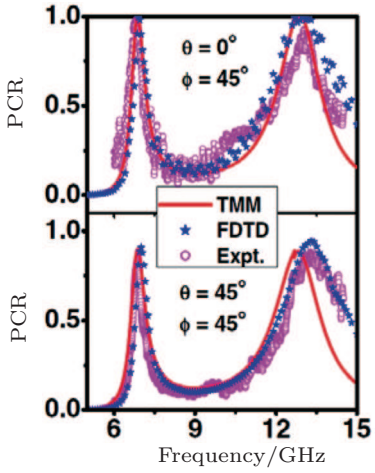


Fig. 2. PCR as the functions of frequency, obtained by TMM calculations on the model system (solid lines), FDTD simulations on the realistic structures (solid stars), and experimental measurements (open circles). The incident direction is (a) $\theta = 0°, \phi = 45°$ and (b) $\theta = \phi = 45°$.[29]

The physics underlying these unusual phenomena can be understood by a simple argument. Consider the normal incidence case for simplicity. Supposing the incident wave is given by $\boldsymbol{E}^{\rm i} = (E_x\hat{\boldsymbol{x}} + E_y\hat{\boldsymbol{y}})\,{\rm e}^{{\rm i}(-\omega z/c+\omega t)}$, then after reflection by an ordinary material, the reflected wave is usually written as $\boldsymbol{E}^{\rm r} = r(E_x\hat{\boldsymbol{x}} + E_y\hat{\boldsymbol{y}})\,{\rm e}^{{\rm i}(\omega z/c+\omega t)}$ with r being the reflection coefficient. However, in the present case with anisotropy ($\mu_{xx} \neq \mu_{yy}$), the reflection coefficients r_x and r_y are different for incident waves polarized along two directions. Thus, in general, the reflected wave should be $\boldsymbol{E}^{\rm r} = E_0\,(r_x\hat{\boldsymbol{x}} + r_y\hat{\boldsymbol{y}})\,{\rm e}^{{\rm i}(\omega z/c+\omega t)}$ and the polarization state can be manipulated through varying r_x and r_y. For the configuration studied in Fig. 2(a) with $E_x = E_y$, if we tune the material parameters to yield $r_x/r_y = -1$, the polarization direction of the reflected wave would be $-\hat{\boldsymbol{x}} + \hat{\boldsymbol{y}}$, which is perpendicular to that of the original wave. A complete polarization conversion (CPC) is thus realized. The key issue is then how to control r_x and r_y. With a metal plate on the back, our structure is always totally reflecting, i.e., $|r_x| = |r_y| \equiv 1$. However, the phase $\Delta\psi$ of the reflection coefficient, defined as $r_{x(y)} = {\rm e}^{{\rm i}\Delta\psi_{x(y)}}$, strongly depends on the metamaterial parameters. We find that in most cases where μ_{xx} (μ_{yy}) is not large, we have $\Delta\psi_{y(x)} \sim \pm 180^\circ$, since the metamaterial layer is transparent and light can directly "see" the metal plate, which is reflecting out of phase. However, at the resonances where μ_{xx} (μ_{yy}) $\to \pm\infty$, we obtain $\Delta\psi_{y(x)} = 0$ since light is reflected directly by the opaque metamaterial which possesses an infinite impedance. In general, we can obtain any value of $\Delta\psi_{y(x)}$ through adjusting the value of μ_{xx} (μ_{yy}) and d. In a word, near each resonance, one of μ_{xx} and μ_{yy} becomes very large while another is close to 1, and thus there must be a frequency where $\Delta\psi_x - \Delta\psi_y = \pm 180^\circ$ and thus $r_x/r_y = -1$.

We employed experiments and FDTD simulations[31] to demonstrate these predictions. To realize the proposed model system shown in Fig. 1(a), we designed and fabricated a sample based on a frequency-selective structure as shown in Fig. 1(b), which consists of a periodic array of planar H-shaped metallic patterns (lattice constant $a = 7$ mm, thickness $d = 0.1$ mm), printed on a 1.2 mm thick PCB slab (with $\varepsilon_{\rm r} = 3.6$) with a metal sheet as substrate. Other structural parameters are fixed as $b = 5$ mm, $w = 1.0$ mm. As a result, the entire structure exhibits magnetic responses with well-defined resonance frequencies, but its electric polarization is strongly diminished since the two currents effectively cancel each other. The composite material is then perfectly described by the double-layer model shown in Fig. 1(a), with d =1.3 mm being the thickness of the H-pattern (0.1 mm) plus the inner dielectric layer (1.2 mm). As schematically shown in Fig. 1(c), the measurements were carried out in an anechoic chamber using a network analyzer (Agilent 8722 ES) and two linearly polarized horn antennas, with the sample rotated and tilted appropriately to achieve a desired incidence angle (θ, φ). As shown in Figs. 2(a) and 2(b), quantitative agreements are found among the results obtained by TMM, FDTD simulations, and experiments. In particular, both experiments and simulations verified the CPC effects predicted by the model analysis. We also found a good agreement between the FDTD simulations and the model TMM results on the relative phase ($\Delta\varphi_{\rm sp}(f)$), which indicates that we can obtain any EM wave polarization desired. We finally employed experiments and simulations to study the angle dependencies of the polarization conversion effects, and satisfactory agreements with the model TMM results were noted.

In 2009, we further pushed this idea to the optical regime with an experimental demonstration, measuring 96% polarization conversion efficiency from s- to p-polarization after reflection, at the working wavelength of 685 nm.[32] Our simulations and analytical results, which are in reasonable agreement with the experimental results, reveal that the underlying physics are governed by the particular electric and magnetic resonances in the optical metamaterial. Based on a similar idea, a broadband plasmonic half-wave plate in reflection has been realized in the near-infrared regime.[33,34]

2.1.2. Transmission geometry

While reflection-type devices have enabled highly efficient polarization control based on ultra-thin systems, they have also suffered the interference issues which are typical for such devices. We solved this issue in 2011. We proposed a transparent anisotropic ultrathin MTM to control the polarization efficiently, including polarization conversion and rotation.[35] Compared to other proposed MTM polarization-control devices in transmission geometry,[36,37] our device does not suffer the energy loss issues.

Figure 3(a) schematically depicts our proposed system, which is a laterally anisotropic ABA tri-layer structure, in which layer A is an electric metamaterial with periodically arranged resonant microstructures, while layer B is a metallic mesh. This design is motivated by a previous study in which a series of perfect transmission peaks were found in a laterally isotropic ABA system.[38] The idea is to utilize the lateral anisotropy to purposely realize perfect transmittance for both incident polarizations at a common frequency but with different transparency mechanisms. When the transmission phase difference for two polarizations is significant, the polarization control can be easily and efficiently realized.

We performed full-wave numerical calculations using a finite-element method (FEM)[39] on realistic structures and TMM calculations on homogeneous slabs[38] to study the transmission properties of the proposed system. Based on the effective media theory, the individual A and B layers can be considered as homogeneous dielectric slabs with $\varepsilon_{\rm A}^x =$

$20.2 + 1917/\left(5.47^2 - f^2\right)$ and $\varepsilon_B = 4.483 - 623.1/f^2$, with f denoting the frequency measured in GHz. Figure 4(a) depicts the transmission spectrum of the system based on FEM simulations for the x-polarization case. By careful analysis, we found that the first two peaks are induced by the perfect EM wave tunneling effect in ABA systems with a mechanism described in Ref. [38] (called "EMT peaks"). For the third peak, we found that it is governed by the extraordinary optical transmission (EOT) mechanism.[40] Since ε_B is negative, the B layer supports surface plasmon polaritons (SPP). However, such modes cannot be directly excited by propagating waves, due to the wavevector mismatch. Fortunately, the A layer can provide a reciprocal vector to compensate for the wave-vector mismatch so that the SPP modes can be "seen" by the incident plane waves, leading to the EOT phenomenon.

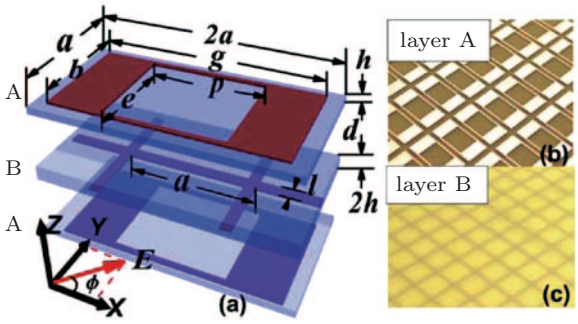


Fig. 3. (a) Unit cell structure of our design: $a = 12$, $b = 10$, $g = 21.3$, $e = 9$, $p = 11$, $l = 1$, $h = 0.6$, and the metal thickness is 0.018, with all lengths measured in units of mm. All substrates have $\varepsilon = 3.5$, and for the B layer, the metallic mesh is sandwiched by two identical substrates. Pictures of fabricated (b) A layer and (c) B layer.[35]

Understanding the physical mechanisms can help us manipulate these transmission peaks freely and independently. The two EMT peaks are dictated by the micro-structure of layer A but are insensitive to the periodicity, while the EOT peak is essentially determined by the periodicity of layer A. Simultaneously, three peaks also exist for a y-polarized incident wave but at different frequencies. Therefore, we purposely adjusted the structure (microstructure, periodicity, d, etc.) to make the EOT peak for x-polarization coincide with the second peak for y-polarization. The transmission spectra (including amplitudes and phases) through the optimized system are shown in Fig. 4 as solid lines for both incident polarizations. We note that the system is perfectly transparent for both polarizations at ~ 5.1 GHz. Meanwhile, the transmission phase changes are $\varphi_x \sim 0^\circ$ and $\varphi_y \sim 90^\circ$ for the two polarizations. The physics underlying such a big difference is that the transparencies are dictated by different principles. For x-polarization, the transparency is the EOT type and thus φ_x is nearly 0, since the role of the A layer is to provide a reciprocal vector, and it does not need to have a large permittivity. In contrast, the transparency for y-polarization is the EMT type (see Fig. 4(b)), so φ_y must be large, since a large permittivity is required for the A layer to compensate for the negative permittivity of the B layer based on the EMT.[38] Such a big $\Delta\varphi$ is remarkable, recalling that our system is only $\lambda/20$ thick. In contrast, the ordinary polarization-modulation materials need to be much thicker than the wavelength to achieve such a phase difference.

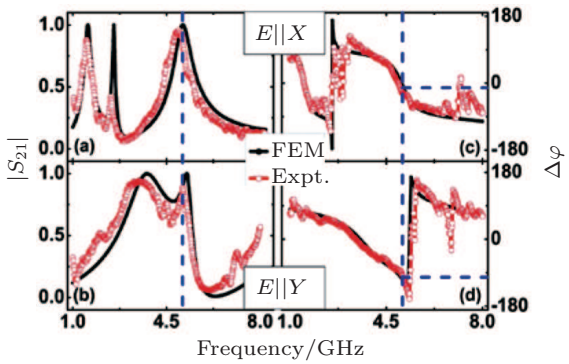


Fig. 4. For the optimized structure (the same as Fig. 1 and with mm), simulated (lines) and measured (circles) spectra of transmission amplitudes and phases for two incident polarizations.[35]

Microwave experiments were performed to verify the theoretical predictions. We fabricated metamaterial samples in sizes 48 cm×48 cm based on the designs (see pictures for A and B layers in Figs. 3(b) and 3(c)) and measured the transmission spectra of the ABA structure using a vector network analyzer (Agilent E8362C PNA). The measured $|S_{21}|$ and $\Delta\varphi$ are plotted as open circles in Fig. 4 for two incident polarizations. Excellent agreement is found between experiment and simulation results. In particular, experiments confirmed that the transmittance is maximized for both polarizations around 5.1 GHz but with a phase difference $\sim 90^\circ$. However, the maximum transmissions cannot reach 100% as predicted by the theory, probably due to imperfections in the sample and the loss in the substrate. We also demonstrated experimentally three typical polarization control effects: linear-to-circular conversion, linear-to-elliptical conversion, and polarization direction rotation.

Note that all the approaches introduced here can be extended to other frequency domains such as the THz, infra-red, and optical regimes,[32,33,41] although the fabrications are far more challenging and the loss issues should be carefully considered.

2.2. Transparency control

Induced high transmittance of EM waves through opaque media has always been fascinating. Such a phenomenon is typically associated with the excitation of some kind of resonance, such as SPPs enabled by the Bragg scattering of periodical structure[42,43] or Fabry–Perot (FP) resonances.[44,45] In 2005, we demonstrated a novel transparency mechanism,[38] different from the SPP-aided[42,43,46] and the FP[44,45] ones,

to make an optically opaque medium (slab B with negative ε, as shown in Fig. 5) perfectly transparent by sandwiching this opaque slab between two identical A slabs with high ε, which are also nearly opaque. For such an ABA structure, we found the following rigorous criterion for perfect transmission:

$$\left(\frac{k_1}{k_0}-\frac{k_0}{k_1}\right)2\tan(k_1d_1)-\left(\frac{\alpha_2}{k_0}-\frac{k_0}{\alpha_2}\right)\tanh(\alpha_2d_2)$$
$$-\left(\frac{k_1^2}{\alpha_2k_0}+\frac{\alpha_2k_0}{k_1^2}\right)\tan^2(k_1d_1)\tanh(\alpha_2d_2)=0,$$

with

$$k_l=\sqrt{\varepsilon_l}\frac{\omega}{c},\qquad k_2=\mathrm{i}\alpha_2.$$

Figures 5(a) and 5(b) show the field patterns for the two $T=1$ solutions. In both cases, we found exponentially growing evanescent waves inside the B layer to completely compensate the usual exponentially decaying wave, resulting in perfect transmissions. We found the magnetic fields to be strongly enhanced around the A–B interfaces, which is a characteristic feature of this phenomenon but not found in others. On the other hand, the electric field is diminished inside the B layer. After considering the phase, we found the magnetic field pattern to exhibit odd symmetry with respect to the center plane of layer B for the EMT-derived solution, and even symmetry for the second solution. A phase diagram is given in Fig. 5(c) to show the maximum enhancement of magnetic field with respect to parameters ε_2 and d $(=d_1=d_2)$ for the EMT-derived transmission. The field enhancement is stronger with larger ε_2 and appropriate d, in clear contrast to the EMT applicable region. Microwave experiments based on MTMs and FDTD simulation were performed to demonstrate such an effect. The overall agreement among the experimental results, the simulation results, and the theory is quite good. In particular, near the critical thickness, experiments do show near 100% transmission at the frequency predicted by the theory. The two properties associated with this transparency, high magnetic field and incident angle independence, were also verified by the FDTD simulations. The present effect is also realizable in infrared or optical regimes with appropriate designs. Based on our idea, unitary transmission through tunnel barriers in Terahertz[47] and optical regimes[48] has been shown to be possible. However, direct scaling of such MTMs to the optical regime is proven invalid, due to the saturation effect of an *LC* resonator at high frequency.[49]

In 2012, we extended our ABA approach to establish a scattering-cancellation mechanism (SCM) to make continuous plasmonic metal transparent.[50] Such a scheme can in principle be realized in the optical frequency domain, since it does not involve *LC* resonators, which suffer the saturation effect. In addition, such a scheme is totally different from the transparency mechanisms with the help of certain resonances such as SPPs[43] or FP resonances.[44] In both the SPP and FP schemes, the targeted metals should be perforated with holes or slits. Moreover, the SPP approach is sensitive to structural order while the FP one requires samples with thicknesses comparable to wavelength, and both are inconvenient for practical realizations. In contrast, our scheme has overcome these problems, since it retains the full electric and mechanical properties of a natural metal (without making holes in the metal) and the transparency is robust against structural disorder and incidence angle.[50]

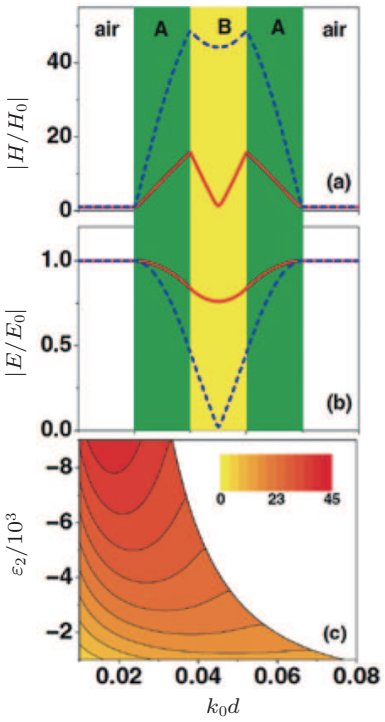


Fig. 5. The (a) $|H/H_0|$ and (b) $|E/E_0|$ as the functions of position for the EMT-derived solution (solid line) and the other solution (dashed line). Here $\varepsilon_2=-2000$, $k_0d=0.02$. (c) Maximum magnetic field enhancement obtained in the EMT-derived perfect transmission state with respect to ε_2 and d.[38]

Figure 6(a) schematically depicts our proposed structure of the transparent conducting metals (TCMs), in which the target continuous metal film C (with thickness h_C and relative permittivity ε_C) is sandwiched by two identical composite layers (with thickness h_{AB}) consisting of alternating dielectric (A) and metallic (B) stripes. To avoid electric shorting, the C layer is separated from the A and B layers by small gaps (with thickness h_a) filled with a medium with relative permittivity ε_a. As a pure theoretical model, we set $\varepsilon_C=-110$ and performed full-wave simulations based on the FEM[39] to compute the transmittance (T) of the whole structure under illuminations of an x-polarized normally incident light. We depict in Fig. 6(b) how T depends on two parameters ε_B and $P=w_A+w_B$ (through varying w_A only), with other parameters fixed as $\varepsilon_A=12$, $w_B=0.1\lambda$, $h_{AB}=h_C=0.02\lambda$, $\varepsilon_a=1$, $h_a=0.01\lambda$, where λ is the incident wavelength. Although a stand-alone C layer is nearly opaque (with $T<2\%$), we note

that such a sandwich structure can be perfectly transparent under certain conditions. The upper high-T band at $P \sim \lambda$ is very narrow, and is easily identified as the EOT band.[40] The lower high-T band is much broader, with governing physics explained by the SCM theory. We applied a mode-expansion theory to analytically solve the scattering problem of the present system.[51,52] The analytical model shows that if the reflection from the AB layer is strong enough to cancel the reflection from the C layer, which is always highly reflective, the whole system can still be perfectly transparent. Since ε_A and ε_B have opposite signs, by adjusting the AB structure one can tune the effective impedance Z_{AB} very efficiently, and in turn, tune the scatterings from two AB layers, so that the perfect transparency condition can be exactly satisfied. Obviously, such a scattering cancellation mechanism needs no structuring of the metal C, so full DC conductivity of metal C can be retained.

We designed realistic TCMs based on Fig. 6(a) in which both C and B are assumed to be Ag, material A is air and the interlayer materials are Al_2O_3. We found the transmittance to be as high as 90% and 75% for an $h_C = 25$ nm and $h_C = 40$ nm design, at 776 nm and 700 nm, respectively. Note that the transmittance through a bare Ag layer of 25 nm thickness is less than 3%.

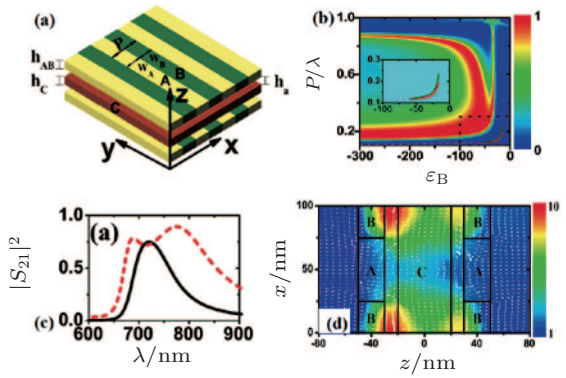


Fig. 6. (a) Geometry of the structure studied in this paper. (b) FEM calculated transmittance through the structure as functions of ε_B and P/λ. Inset shows a zoomed view of the rectangular region. (c) FEM calculated transmission spectra of the designed TCMs (solid line for $h_C = 25$ nm and dashed line for $h_C = 40$ nm) with other parameters $\varepsilon_A = 1, \varepsilon_a = 3.06$, and $h_a = 10$ nm. (d) Distributions of normalized H-field (color-map) and energy flux (arrows) inside the $h_C = 40$ nm structure under the illumination of an x-polarized light at $\lambda = 726$ nm.[50]

We performed proof-of-concept experiments in the microwave regime to verify the proposed scheme. In microwaves, metals behave as perfect conductors and do not exhibit finite negative ε. However, metallic meshes with subwavelength openings are shown to exhibit Drude-like ε in the microwave regime,[1] and therefore are chosen to mimic the plasmonic metals B and C at optical frequencies. Figures 7(a) and 7(b) show that the measured spectra are in excellent agreement with FEM simulations for layer B and layer C with effective permittivity $\varepsilon_B = 5 - 580/f^2$ and $\varepsilon_C = 5 - 2300/f^2$ (f denoting the linear frequency measured in GHz). Figure 7(c) depicts the measured and simulated transmission spectra through such an ABC structure, where a transparent band is identified at ~4.4 GHz with peak transmittance ~100%! This is quite counter-intuitive at first glance, since when bare, such a layer C is nearly opaque (with $T < 5\%$). The experimental and simulated results shown in Figs. 7(d) and 7(e) demonstrate the incidence angle-independence properties of the SCM transparency, which are very useful for real applications. We also found that our mechanism is quite robust against the structural disorder.

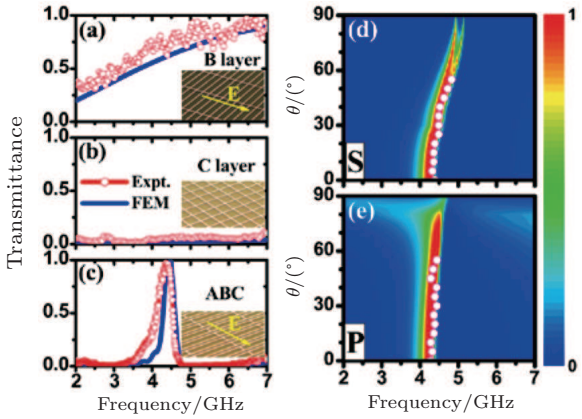


Fig. 7. Measured (open circles) and simulated (solid lines) transmission spectra of (a) layer B, (b) layer C, and (c) the designed ABC structure. FEM-calculated transmittance as functions of incident angle and frequency for (d) s- and (e) p-polarized incident waves, with open circles representing the measured maximum-transmittance positions.[50]

Again, such an idea can in principle be realized in high-frequency domains. In fact, we have realized a transparent electrode in the THz regime by extending the symmetrical ABA structure to an asymmetrical configuration.[53] A similar idea was also proposed to make anti-reflective coatings in the THz regime.[54]

3. Plasmonic MTMs for SPP control and their applications

SPPs attracted considerable attention recently.[42,43,46,55] The plasmon frequency ω_p of a natural material is fixed by its electron density, which limits the applications significantly. In 2004, Pendry *et al.* demonstrated that a metallic plate with periodic square holes can mimic a plasmonic material in terms of SPP properties,[52] with effective ω_p dictated by the structure.[51] However, to make the idea work, one has to fill the holes with high-index materials, which is not easy to realize in practice, particularly at higher frequencies.

Attracted by the multiband and subwavelength properties of fractals, several groups investigated the rich EM wave characteristics of various fractal structures.[56,57] Inspired by such prior work, we found that a metallic plate drilled with fractal-shaped slits (see Fig. 8(a)) exhibits SPPs with ω_p dictated by the fractal geometry.[58] Without using high-index

insertions[51,52] and distinct from the narrow rectangular hole case,[59] the system can be homogenized as a plasmonic metamaterial to support transverse-magnetic (TM) and transverse-electric (TE) SPPs simultaneously, due to a subwavelength property of the fractal pattern along all dimensions at resonance. Most importantly, the effective plasmon frequency of such a system can be changed via adjusting the fractal geometry. Therefore, we can in principle design a plasmonic metamaterial at any desired frequency. These plasmonic MTMs can support many interesting applications. In what follows, we will introduce two typical applications of such structures, including super and hyper imaging, and slow-wave metasurfaces to enhance light–matter interactions.

3.1. Super and hyper imaging

Now that such a system supports well-defined SPPs, it is natural to expect that we can use it to focus light sources with all subwavelength resolutions. We designed and fabricated plasmonic MTMs in the microwave regime (see Fig. 8(b) for the sample picture and the unit cell structure), and performed microwave experiments to demonstrate the super imaging effects. Putting a small antenna on the front surface of a slab of our MTM, we employed another, identical antenna to measure the field distribution on the exit surface of the lens. Both measurements and FDTD results show that the images focused by our lenses (with different thicknesses) are only ~ 8 mm wide, which are $\sim \lambda/15$ since the working wavelength is $\lambda \approx 119$ mm. In contrast, images formed without lenses (solid squares) do not show any subwavelength resolutions at all. In addition, the field strength is enhanced when a lens is added. The subwavelength resolution and enhanced field strength are two important characteristics of the SPP.[43,55]

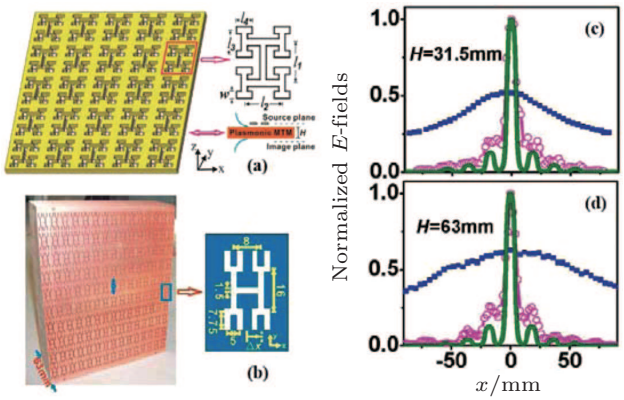


Fig. 8. (a) Geometry of the fractal plasmonic MTMs. Unit cell's parameters measured in μm : $l_1 = l_2 = H = 0.5$, $l_3 = l_4 = 0.25$, $w = 0.06$. (b) Picture of a 63-mm-thick fractal plasmonic metamaterial and its unit cell structure (all lengths are measured in mm). Here the periodicity is 18 mm (32 mm) in the x (y) direction. (c) and (d) Electric field distributions along the line perpendicular to the antenna on the image plane obtained by experiments (open circles) and FDTD simulations (solid lines) for different lens thickness, referenced by the experimental results measured without any lens (solid squares). Here, the maximum electric field is normalized to 1 in the presence of a lens.[58]

We further investigated the role of the aperture shape on super imaging effect with such metallic plasmonic MTMs.[60] Through analyzing the transmission properties of metallic plates with different apertures, we found two conditions for such structures to work as super lenses. First, the working wavelength dictated by the aperture's shape resonance should be much larger than the array's periodicity. Second, the coupling strength $|S_0|$ between the aperture's fundamental waveguide mode and external radiations should be as small as possible. These two conditions contradict each other for a square-shaped aperture, so high index materials should be inserted into the apertures, while a fractal-shaped aperture satisfies these two conditions simultaneously without using high-index insertions. Numerical simulations were performed to illustrate the imaging properties of these plasmonic lenses.

Such an amazing super-imaging property of our plasmonic MTM can be interpreted in a different way. We demonstrated that our system can optically well mimic the optical-null medium (ONM),[61] which is a particular type of TO medium representing an optically non-existant space. According to the TO theory,[8,9] the ONM is obtained by expanding a zero-thickness space to a finite-thickness slab and exhibits the following EM parameters (in Cartesian coordinates):

$$\varepsilon = \mu = \begin{pmatrix} 0 & 0 & 0 \\ 0 & 0 & 0 \\ 0 & 0 & \infty \end{pmatrix}.$$

Therefore, an ONM can transfer any wave from its front surface to its exit surface perfectly without any phase accumulations, as if the ONM does not exist at all. FEM[39] simulations clearly demonstrated this peculiar property of the ONM (see Fig. 9).

We derived an effective-medium theory (EMT) based on the rigorous mode expansion theory[51] to homogenize our plasmonic MTM. At the working frequency, which is just the waveguide cut-off of the aperture, we found the effective ε and μ of our system can be expressed by

$$\varepsilon_{\text{eff}} = \varepsilon_0 \begin{pmatrix} 0 & 0 & 0 \\ 0 & 0 & 0 \\ 0 & 0 & \infty \end{pmatrix}, \quad \mu_{\text{eff}} = \mu_0 \begin{pmatrix} |S_0|^2 & 0 & 0 \\ 0 & |S_0|^2 & 0 \\ 0 & 0 & \infty \end{pmatrix},$$

where $|S_0|^2$ is the coupling strength mentioned previously. Therefore, if we can design a system exhibiting such a plasmonic MTM (at the frequency) then it can well mimic an ONM optically. Full-wave simulation results justified this argument based on a carefully designed plasmonic MTM.[61] It is thus very natural to understand why such a system can work as a super lens.

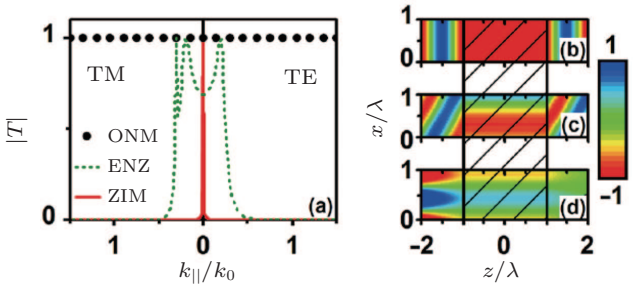


Fig. 9. (a) FEM-computed transmission amplitudes $|T|$ for EM waves with different incident angle and polarization passing through a 2λ-thick slab of ONM (solid circles), epsilon-near-zero medium (ENZ, green dash line, with $\varepsilon = 0.1$) or zero-index-material (ZIM, red line), correspondingly. (b)–(d) FEM simulated electric field (E_y) distributions for TE-polarized EM waves passing through a 2λ-thick ONM slab with parallel wave vectors: (b) $k_x = 0$, (c) $k_x = 0.5k_0$, and (d) $k_x = 1.2k_0$. Here, the wave vector is in a vacuum, and the shadow areas represent the ONM.[61]

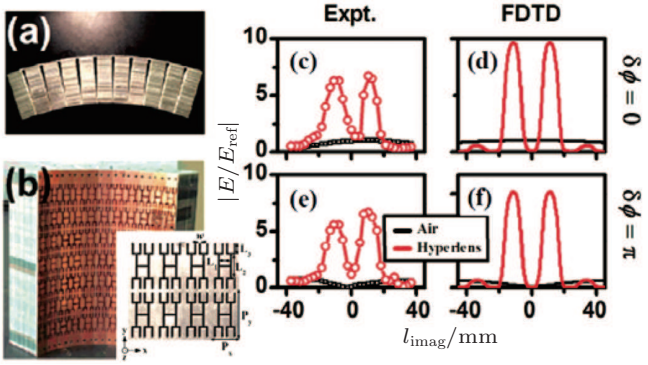


Fig. 10. (a) Top-view and (b) side-view pictures of the experiment sample. Inset shows the picture of the fabricated sample with parameters (in mm): $L_1 = 12$, $L_2 = 13$, $L_3 = 6$, $P_x = 18$, $P_y = 31$, $w = 1$. (c), (e) Measured and (d), (f) simulated $|E/E_{ref}|$ distributions at the outer surface of the hyperlens when two dipole antennas are placed on the inner surface of the hyperlens, fed by in-phase ((c) and (d)) and out-of-phase ((e) and (f)) signals. Black lines/symbols correspond to the case of replacing the sample by air. In both measurements and simulations, the $|E|$ value at the position $l_{imag} = 0$ mm in the in-phase case is taken as the reference $|E_{ref}|$.[61]

The ability to mimic an ONM opens up more applications for our plasmonic MTMs. For example, after bending a slab of ONM to a curved shape, the new system must work as a hyper lens, which can not only focus a light source but also magnify the image size. As shown in Fig. 10, we performed microwave experiments at working frequency 2.63 GHz to demonstrate the hyperlensing effect with a designed realistic sample. Put two point sources separated by a deep-subwavelength distance 18 mm, we found that the two point sources can be clearly distinguished on the image plane, with measured half-maximum width of each peak being roughly 20 mm $\sim \lambda/6$. More importantly, now the separation of the two peaks is 23 mm, which is enhanced by a factor of ~ 1.3 as compared to the original value 18 mm, and the field at the image peak is enhanced significantly better (more than 7 times) than that without the hyperlens. All these features are consistent with the theoretical predictions based on an ONM. Two things are worth mentioning here. First, our experiments demonstrate that the hyperlensing effect is independent of $\delta\varphi$ (see Figs. 10(c) and 10(e)), which is the desired result, according to the "stretching" operation. Such an interesting property offers the ONM more freedom for future applications. Second, although the magnification factor is only ~ 1.3 in the present demonstration, this factor can be easily improved by increasing the curvature or the thickness of our device.

3.2. Slow-wave meta-surfaces to enhance light–matter interactions

We can even construct a slow-wave meta-surface by putting such a plasmonic MTM on top of a dielectric spacer backed by a metallic sheet. The whole device is still much thinner than wavelength, yet it can support slow wave propagations along all directions and allow a perfect coupling between inner slow-wave modes with external fast waves.[62] Such a slow-wave mechanism is very different from available approaches, such as the Bragg mechanism in photonic crystals,[63] the electromagnetically induced transparency (EIT) mechanism in atomic gases,[64] photonic systems with negative-refraction MTM components,[65,66] and Fano resonance-based MTMs.[67,68]

Our sandwich structure is schematically shown in Fig. 11(a). We first experimentally measured the reflection time delay (ΔT) of a microwave pulse incident from air onto our system. The time that the pulse travels in air is deduced, so that ΔT precisely measures the net time in which the pulse is trapped inside the structure. The $\Delta T(\omega)$ spectrum deduced from experimental data is depicted in Fig. 11(b), which is in excellent agreement with simulation results based on the FEM.[39] We noted that while $\Delta T \approx 0$ at most frequencies, ΔT significantly increases in a frequency window centered at ~ 5.5 GHz, indicating that our structure can trap the EM pulse for a long time. With the FEM simulation at three typical frequencies, shown in the inset of Fig. 11(b), the noted phenomena can be easily understood: while EM waves are directly reflected back by the upper surface at both 4 GHz and 7 GHz, they could penetrate inside the apertures at 5.5 GHz and stay there for a long time (~ 2 ns) before leaving the structure. The effective wave speed inside our structure is

$$v_g = 2h/\Delta T \sim c/100$$

at ~ 5.5 GHz. The slow-wave effect is robust against the polarization and the incident angle of the input beam, and similar spectra were obtained for TE-polarization cases with different incident angles. Figure 11(c) depicts how ΔT depends on two parameters h_1 and h_2, obtained by FEM simulations. In the

left corner, where both h_1 and h_2 are large, ΔT depends linearly on h_1 and h_2, suggesting the dominance of a bulk effect. Intriguingly, as h_1, $h_2 \to 0$, ΔT does not decrease but rather increases dramatically. The common linear dependencies exhibited by the two curves in the region $h_1 > 10$ mm suggest an analytical formula for

$$\Delta T \approx \Delta T_s + 2h_1/v_z.$$

We note that each aperture in the upper metallic plate forms a waveguide as h_1 becomes large, and therefore, v_z precisely represents the group velocity for photons traveling inside such a waveguide. On the other hand, the term ΔT_s, which does not depend on h_1, must be a surface-related remaining contribution. Our FEM simulations and microwave experiment verified such anomalous behaviors of ΔT_s in small-h regions.

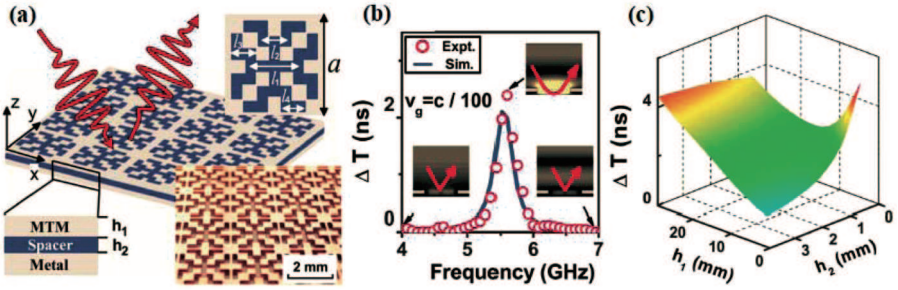


Fig. 11. (a) Geometry of the designed meta-surface and picture of part of a fabricated sample with $a = 20$, $w = 2$, l_1=10, $l_2 = l_3 = l_4 = 5$, h_1=$h_2 = 2$ (measured in mm). The metallic material used here is copper, and the spacer is just an air gap. (b) Measured (red dot) and simulated (blue lines) delay time spectra for the fabricated meta-surface. Insets show the calculated electric-field distributions under external radiations at different frequencies. (c) FEM-simulated delay time (calculated at frequency 5.5 GHz) as a function of h_1 and h_2 with other geometrical parameters the same as those in panel (a).[62]

We found the physics of such an anomalous effect arise from the enhanced mode-hybridization effect. In our system, the incoming EM wave first excites the spoof SPPs, which propagate very slowly on the structural surface. It takes a very long time ($\sim \Delta T_s$) for the SPP wave to penetrate into the waveguides since each aperture has a very small opening. Wave propagation inside the waveguide is again very slow since $v_z \ll c$ here, resulting in an additional delay time $\sim h_1/v_z$. For the system with small h_1 and h_2, ΔT is mainly contributed by the surface term ΔT_s. We found that the stronger mode-hybridization in the smaller h_2 case results in stronger local field enhancement, with the longer surface delay time ΔT_s. This explains the singular dependence of the slow-wave effect on h_1 and h_2, as observed in our structure. As a result, our system has a larger Purcell factor ($\sim Q/V$) than the FP one, leading to better performance in enhancing the LMIs.

Such a slow-wave meta-surface can have many applications, especially in enhancing light–matter interactions (LMI). We first took light-absorption as an example. Inserting low-absorptive FR4-PCB powders (with $\varepsilon = 1.5 + 0.03\mathrm{i}$) into the apertures and replacing the air-gap by a 2-mm-thick low-absorptive dielectric spacer (with $\varepsilon = 3.9 + 0.075\mathrm{i}$), we performed microwave experiments to measure the absorption spectra of the entire system. As shown in Fig. 12, absorbance is significantly enhanced in a frequency window centered at ~4 GHz with peak absorption ~100% for an input wave with TE or TM polarizations at an incident angle $\theta = 15°$. Note that the total thickness of our structure is only $\sim \lambda/20$, and can in principle be further reduced. Simulation results (lines) are in excellent agreement with experiment, both showing that the perfect absorption effect is robust against the polarization, incident angle θ, and azimuthal angle ϕ of the in-plane E vector (see Fig. 12(b)). As another example, we show by full-wave simulations that the third-harmonic nonlinear generation can also be significantly enhanced by putting nonlinearly active materials inside the apertures of our slow-wave structures. Other interesting LMI enhancements can also be expected, and we are looking forward to experimental verifications.

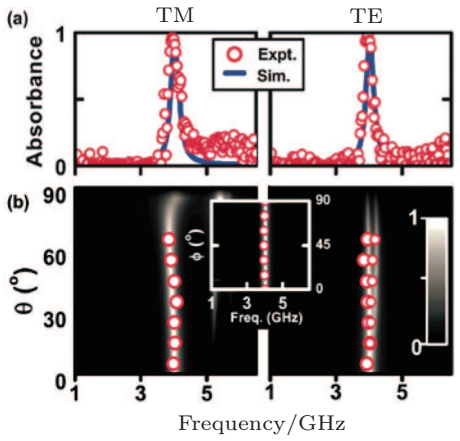


Fig. 12. (a) Measured (circles) and simulated (lines) EM wave absorption spectra under radiations with TM- or TE-polarizations and $\theta = 15°$, $\varphi = 0°$. (b) FEM-computed absorbance versus incidence angle and frequency under radiations with TM- or TE-polarizations and $\varphi = 0°$; circles denote the absorption peak position measured experimentally. Inset shows the measured (circles) and simulated φ dependences of the absorption peak (setting $\theta = 15°$).[62]

4. Inhomogeneous meta-surface for wave-front control

In the above sections, we focused on those MTMs constructed based on simple homogeneous or periodic orders but with different and carefully designed meta-atoms. Recently, inhomogeneous meta-surfaces (ultrathin MTMs) constructed based on specific orders have attracted much attention.[18–20,24] Distinct from the TO devices, which gradually manipulate the propagation phase for light travelling inside the medium, meta-surfaces can locally supply abrupt transmission/reflection phase changes in the deep-subwavelength scale and thus exhibit even stronger abilities to manipulate light propagations. Since EM waves do not need to propagate inside the meta-surfaces for a long time, the energy dissipations are strongly reduced. On the other hand, such devices are typically much thinner than the wavelength, which is another attractive characteristic, compared to the conventional bulky MTMs.

In 2011, Capasso's group proposed the first inhomogeneous meta-surface consisting of V-shaped optical antennas with different sizes and geometries.[18] Each V-shaped antenna is carefully selected to provide an appropriate phase for scattered waves, such that the whole system exhibits a linearly changing phase profile with a constant gradient $\mathrm{d}\Phi/\mathrm{d}x$. When the meta-surface was illuminated by incident light at the working wavelength $\lambda = 8$ μm, the authors experimentally observed anomalously reflected and refracted modes which satisfy the generalized Snell's law

$$\begin{cases} \sin\theta_{\mathrm{t}} n_{\mathrm{t}} - \sin\theta_{\mathrm{i}} n_{\mathrm{i}} = \dfrac{\lambda_0}{2\pi}\dfrac{\mathrm{d}\Phi}{\mathrm{d}x}, \\ \sin\theta_{\mathrm{r}} - \sin\theta_{\mathrm{i}} = \dfrac{\lambda_0}{2\pi}\dfrac{\mathrm{d}\Phi}{\mathrm{d}x}, \end{cases}$$

derived from Fermat's principle. Here, θ_{i}, θ_{r}, and θ_{t} denote the incident/reflection/refraction angles, respectively, and n_{i}, n_{t} denote the refraction indices for two different media sandwiching the meta-surface. The idea was soon pushed into the near-infrared regime (~ 2 μm) by Shalaev's group, who further demonstrated experimentally that such an effect is quite a broadband.[19]

However, such meta-surfaces suffer two shortcomings. First, the polarization of the anomalous reflection/refraction modes has been changed with respect to that of the incident beam (Fig. 13(b)). Second, for such systems, normal reflection/refraction modes are also observed (Figs. 13(c) and 13(d)) so that the efficiency of anomalous reflection/refraction cannot be high. In 2012, our group introduced a new class of meta-surface to overcome these two shortcomings.[20] In addition, we experimentally demonstrated that such a new type of meta-surface can serve as a bridge to link propagating waves (PWs) and surface waves (SWs).[20] The structure consists of various H-shaped resonators and a metal sheet, separated by a thin dielectric spacer. Obviously, our meta-surface works in reflection geometry and prohibits the channels for all transmission modes. For different meta-atoms, the reflection amplitudes are always 100% and the reflection phases are carefully designed to satisfy a linear distribution with a constant gradient ξ. We found that reflections by our meta-surface satisfy the generalized Snell's law $k_x = \xi + k_0 \sin\theta_{\mathrm{i}}$, indicating that the meta-surface provides an additional wave vector $\xi = \mathrm{d}\Phi/\mathrm{d}x$ to the incident beam. In addition, both theoretical calculations (including mode-expansion theory[19] and FDTD simulations) and experiments demonstrate that the normal (specular) mode is totally suppressed and the incident PWs can be converted to the anomalous reflection mode with nearly 100% efficiency. As ξ is larger than k_0 or the incident angle is larger than a critical value ($\theta_{\mathrm{ic}} = \sin^{-1}(\sin 90^o - \xi/k_0)$), the reflected beam will become an SW since its parallel wave vector k_x is larger than k_0. Our theoretical prediction for the PW–SW conversion has been experimentally demonstrated by near field measurements (see Fig. 14). Distinct from the conventional PW–SW couplers such as prism or grating couplers, here our meta-surface works with a non-resonant coupling nature and thus supports a highly efficient PW–SW conversion for a wide range of incident angles.[20] Compared with the meta-surfaces introduced by Capasso's group, our systems exhibit much-enhanced efficiency for polarity-conserved anomalous reflection and can serve as the very bridge to link PW and SW. We soon realized the idea in the optical regime, and the fabricated meta-surface exhibits a $\sim 80\%$ efficiency for anomalous reflection within a broad range of wavelengths (750 nm–900 nm).[24]

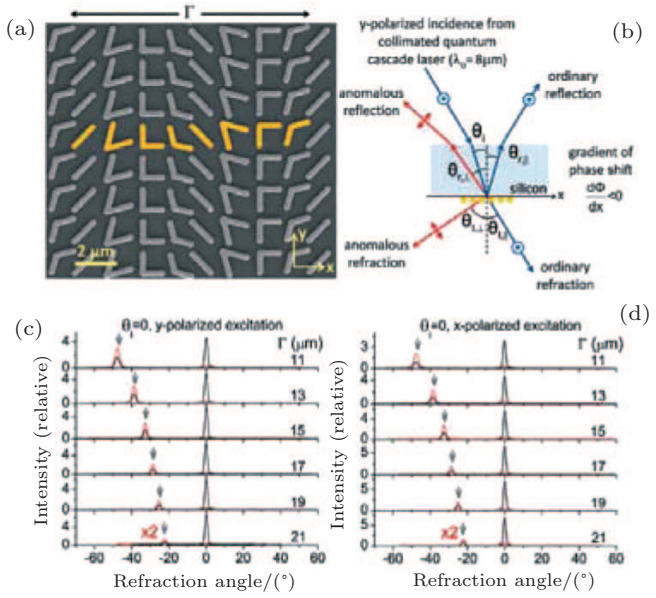


Fig. 13. (a) SEM image of one representative meta-surface to demonstrate generalized Snell's law. (b) Schematic experimental setup of ordinary and anomalous reflections/refractions under y-polarized excitation. (c) Measured far-field intensity profiles of the refracted beams for y- and x-polarized excitations, respectively, with different unit cell lengths Γ.[18]

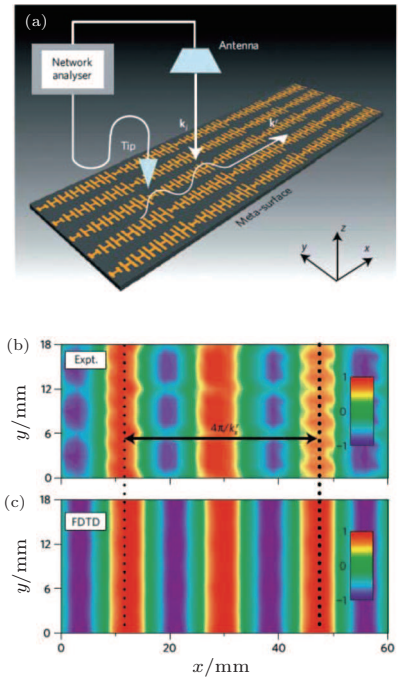


Fig. 14. (a) Schematic picture describing the near field scanning technique. The E_z distributions (with phase information included) on part of the $\xi = 1.14k_0$ meta-surface under illumination of a normally incident x-polarized EM wave, obtained by (b) near-field scanning measurement and (c) FDTD simulations.[20]

The development of meta-surfaces has opened up a new sub-field in MTMs research. Many fascinating effects have been demonstrated based on meta-surfaces, such as directional high-efficiency SPP couplers,[22,23] flat lenses,[25,26,69] the photonic spin Hall effect,[28] meta-holograms,[70] and out-of-plane reflection/refractions.[71] We believe that meta-surfaces can not only serve as an ideal platform for fundamental research, but also find real applications in the near future.

5. Conclusions

In conclusion, we have presented a short overview to summarize our recent work on light manipulations using homogeneous MTMs and inhomogeneous meta-surfaces. We introduced the basic concepts, key properties, experimental verifications, and potential applications of three types of light–manipulation effects, including polarization and transparency controls using the conventional MTMs, SPP controls using plasmonic MTMs, and wave-front controls using inhomogeneous meta-surfaces. We look forward to more exciting new ideas and new developments inspired by this review.

References

[1] Pendry J B, Holden A J, Stewart W J and Youngs I 1996 *Phys. Rev. Lett.* **76** 4773
[2] Pendry J B, Holden A J, Robbins D J and Stewart W J 1999 *IEEE Trans. Microw. Theory Tech.* **47** 2075
[3] Shelby R, Smith D R and Schultz S 2001 *Science* **292** 77
[4] Smith D R, Pendry J B and Wiltshire M C K 2004 *Science* **305** 788
[5] Fang N, Lee H, Sun C and Zhang X 2005 *Science* **308** 534
[6] Zhang X and Liu Z 2008 *Nat. Mater.* **7** 435
[7] Soukoulis C M and Wegener M 2010 *Science* **330** 1633
[8] Leonhardt U 2006 *Science* **312** 1777
[9] Pendry J B, Schurig D and Smith D R 2006 *Science* **312** 1780
[10] Chen H, Chan C T and Sheng P 2010 *Nat. Mater.* **9** 387
[11] Liu R, Ji C, Mock J J, Chin J Y, Cui T J and Smith D R 2009 *Science* **323** 366
[12] Cai W, Chettiar U K, Kildishev A V and Shalaev V M 2007 *Nat. Photon.* **1** 224
[13] Lai Y, Ng J, Chen H, Han D, Xiao J, Zhang Z Q and Chan C T 2009 *Phys. Rev. Lett.* **102** 253902
[14] Jiang W X, Ma H F, Cheng Q and Cui T J 2010 *Appl. Phys. Lett.* **96** 121910
[15] Jiang W X, Cui T J, Ma H F, Zhou X Y and Cheng Q 2008 *Appl. Phys. Lett.* **92** 261903
[16] Jiang W X, Ma H F, Cheng Q and Cui T J 2010 *Opt. Express* **18** 11276
[17] Chen H, Hou B, Chen S, Ao X, Wen W and Chan C T 2009 *Phys. Rev. Lett.* **102** 183903
[18] Yu N, Genevet P, Kats M A, Aieta F, Tetienne J P, Capasso F and Gaburro Z 2011 *Science* **334** 333
[19] Ni X, Emani N K, Kildishev A V, Boltasseva A and Shalaev V M 2012 *Science* **335** 427
[20] Sun S, He Q, Xiao S, Xu Q, Li X and Zhou L 2012 *Nat. Mater.* **11** 426
[21] Xiao S, He Q, Qu C, Li X, Sun S and Zhou L 2013 *Opt. Express* **21** 129
[22] Qu C, Xiao S, Sun S, He Q and Zhou L 2013 *Europhys. Lett.* **101** 54002
[23] Huang L, Chen X, Mühlenbernd H, Li G, Bai B, Tan Q, Jin G, Zentgraf T and Zhang S 2012 *Nano Lett.* **12** 5750
[24] Sun S, Yang K, Wang C, Juan T, Chen W T, Liao C Y, He Q, Xiao S, Kung W T, Guo G Y, Zhou L and Tsai D P 2012 *Nano Lett.* **12** 6223
[25] Li X, Xiao S, Cai B, He Q, Cui T J and Zhou L 2012 *Opt. Lett.* **37** 4940
[26] Gaburro Z and Capasso F 2012 *Nano Lett.* **12** 4932
[27] Huang L, Chen X, Bai B, Tan Q, Jin G, Zentgraf T and Zhang S 2013 *Light Sci. Appl.* **2** e70
[28] Yin X, Ye Z, Rho J, Wang Y and Zhang X 2013 *Science* **339** 1405
[29] Hao J, Yuan Y, Ran L, Jiang T, Kong J, Chan C and Zhou L 2007 *Phys. Rev. Lett.* **99** 063908
[30] Hao J and Zhou L 2008 *Phys. Rev. B* **77** 094201
[31] Simulations were perfomed using the package Concerto 7.0, developed by Vector Fields Limited, England, 2008
[32] Hao J, Ren Q, An Z, Huang X, Chen Z, Qiu M and Zhou L 2009 *Phys. Rev. A* **80** 023807
[33] Pors A, Nielsen M G and Bozhevolnyi S I 2013 *Opt. Lett.* **38** 513
[34] Pors A and Bozhevolnyi S I 2013 *Opt. Express* **21** 2942
[35] Sun W, He Q, Hao J and Zhou L 2011 *Opt. Lett.* **36** 927
[36] Chin J Y, Lu M and Cui T J 2008 *Appl. Phys. Lett.* **93** 251903
[37] Ye Y and He S 2010 *Appl. Phys. Lett.* **96** 203501
[38] Zhou L, Wen W, Chan C and Sheng P 2005 *Phys. Rev. Lett.* **94** 243905
[39] COMSOL Multiphysics 3.5, developped by COMSOL Inc (Burlington, USA, 2008)
[40] Genet C and Ebbesen T W 2007 *Nature* **445** 39
[41] Pors A and Bozhevolnyi S I 2013 *Opt. Express* **21** 27438
[42] Ebbesen T W, Lezec H J, Ghaemi H, Thio T and Wolff P A 1998 *Nature* **391** 667
[43] Barnes W L, Dereux A and Ebbesen T W 2003 *Nature* **424** 824
[44] Porto J, Garcia-Vidal F and Pendry J 1999 *Phys. Rev. Lett.* **83** 2845
[45] Yang F and Sambles J 2002 *Phys. Rev. Lett.* **89** 063901
[46] Martí-Moreno L, García-Vidal F J, Lezec H J, Pellerin K M, Thio T, Pendry J B and Ebbesen T W 2001 *Phys. Rev. Lett.* **86** 1114
[47] Chen H T, O'Hara J F, Azad A K and Taylor A J 2011 *Laser Photon. Rev.* **5** 513
[48] Hooper I, Preist T and Sambles J 2006 *Phys. Rev. Lett.* **97** 053902
[49] Zhou J, Koschny T, Kafesaki M, Economou E N, Pendry J B and Soukoulis C M 2005 *Phys. Rev. Lett.* **95** 223902
[50] Song Z, He Q, Xiao S and Zhou L 2012 *Appl. Phys. Lett.* **101** 181110
[51] Garcia-Vidal F J, Martí-Moreno L and Pendry J B 2005 *J. Opt. A: Pure Appl. Opt.* **7** S97

[52] Pendry J B, Martí-Moreno L and Garcia-Vidal F J 2004 *Science* **305** 847
[53] Malureanu R, Zalkovskij M, Song Z, Gritti C, Andryieuski A, He Q, Zhou L, Jepsen P U and Lavrinenko A V 2012 *Opt. Express* **20** 22770
[54] Chen H T, Zhou J, O'Hara J F, Chen F, Azad A K and Taylor A J 2010 *Phys. Rev. Lett.* **105** 073901
[55] Ozbay E 2006 *Science* **311** 189
[56] Werner D H and Ganguly S 2003 *IEEE Antennas Propag. Mag.* **45** 38
[57] Wen W, Zhou L, Hou B, Chan C and Sheng P 2005 *Phys. Rev. B* **72** 153406
[58] Huang X, Xiao S, Ye D, Huangfu J, Wang Z, Ran L and Zhou L 2010 *Opt. Express* **18** 10377
[59] Shin Y M, So J K, Jang K H, Won J H, Srivastava A and Park G S 2007 *Phys. Rev. Lett.* **99** 147402
[60] Xiao S, He Q, Huang X and Zhou L 2011 *Metamaterials* **5** 112
[61] He Q, Xiao S, Li X and Zhou L 2013 *Opt. Express* **21** 28948
[62] Xiao S, He Q, Huang X, Tang S and Zhou L 2012 *Phys. Rev. B* **85** 085125
[63] Baba T 2008 *Nat. Photon.* **2** 465
[64] Hau L V, Harris S E, Dutton Z and Behroozi C H 1999 *Nature* **397** 594
[65] Tsakmakidis K L, Boardman A D and Hess O 2007 *Nature* **450** 397
[66] Jiang T, Zhao J and Feng Y 2009 *Opt. Express* **17** 170
[67] Zhang S, Genov D A, Wang Y, Liu M and Zhang X 2008 *Phys. Rev. Lett.* **101** 047401
[68] Wu C, Khanikaev A B and Shvets G 2011 *Phys. Rev. Lett.* **106** 107403
[69] Pors A, Nielsen M G, Eriksen R L and Bozhevolnyi S I 2013 *Nano Lett.* **13** 829
[70] Larouche S, Tsai Y J, Tyler T, Jokerst N M and Smith D R 2012 *Nat. Mater.* **11** 450
[71] Aieta F, Genevet P, Yu N, Kats M A, Gaburro Z and Capasso F 2012 *Nano Lett.* **12** 1702